Investigating the metallic behavior of Na clusters using site-specific polarizabilities

Li Ma,[1,*] Koblar Alan Jackson,[2,†] Jianguang Wang,[1] Mihai Horoi,[2] and Julius Jellinek[3,‡]
[1]*Physics Department, Northwest University, Xi'an 710069, China*
[2]*Physics Department, Central Michigan University, Mt. Pleasant, Michigan 48859, USA*
[3]*Chemical Sciences and Engineering Division, Argonne National Laboratory, Argonne, Illinois 60439, USA*
(Received 25 October 2013; revised manuscript received 18 December 2013; published 24 January 2014)

A site-specific analysis scheme based on density functional theory is used to investigate the static polarizability response of Na_N clusters for N up to 80. The cluster structures used in the study stem from extensive searches for the respective global minima. The analysis involves partitioning the total cluster polarizability exactly into site (or atomic) contributions; it also results in the decomposition of the polarizability into local (or dipole) and charge transfer contributions. The computed total polarizabilities are found to be in excellent agreement with recent experimental measurements up to a small overall shift. The site analysis provides clear evidence that interior atoms in sodium clusters are strongly screened from an applied external field by the charge induced at the cluster surface. In addition, cluster size trends in the local and charge transfer contributions are shown to be reproduced very well by a simple metal sphere model. The overall picture is that of clusters exhibiting metallic behavior down to the smallest sizes.

DOI: 10.1103/PhysRevB.89.035429 PACS number(s): 36.40.Cg, 31.15.A−, 33.15.Kr

I. INTRODUCTION

The abiding interest in the behavior of atomic clusters stems from the fact that they are the smallest condensed matter systems. Physical and chemical properties are known to depend sensitively on the number of atoms in the cluster size regime, and systematically investigating the properties of clusters as a function of size yields insight into how bulklike properties emerge at the nanoscale. The electronic properties of clusters are particularly interesting yet challenging to characterize. Since clusters have discrete electron-energy levels, rules based on bulk energy bands cannot be applied. New approaches to understanding the behavior of cluster systems are needed.

The dipole polarizability is a direct measure of a system's response to an applied electric field. Many experimental measurements of polarizabilities have appeared in the literature for various cluster systems [1,2]. These utilize a cluster-beam deflection technique that can yield both the polarizability and the static, zero-field electric dipole moment of a cluster. Cluster polarizabilities and dipole moments can also be computed using the theoretical framework of density functional theory (DFT), allowing for direct comparison with experimental results and providing additional insight into the behavior of the clusters [3–6].

Recently, high precision measurements of cluster polarizabilities and dipole moments were made for sodium clusters (Na_N) [7]. The temperatures of the clusters were reported to be 20 K, so the observed clusters were assumed to be in their ground state structures. A fascinating result of the experiments was that the observed dipole moments for Na_N were found to be vanishingly small for clusters for all sizes down to $N = 3$. This was remarkable since DFT calculations for the likely ground state clusters predicted [8,9] much larger dipoles that should have been observed easily given the precision of the experiments. The absence of permanent dipoles led to the conclusion that Na clusters are metallic down to the smallest sizes [7]. The reasoning was that a metal cannot support a nonzero dipole in its interior; the free electron charge of the metal would rearrange itself to quench any dipole.

More recently, calculations on clusters up to $N = 20$ produced results that suggest a different interpretation of the missing dipoles [10]. In that study, DFT-based molecular dynamics (MD) calculations were performed to simulate the effects of quantum zero point motion (ZPM) on the cluster structures and the corresponding dipoles. The clusters were found to be fluxional, even at the low energies corresponding to ZPM. Because of this, the simulated dipole moments average to nearly zero over a timescale corresponding to the vibrations and would therefore also be effectively zero on the much longer timescale of the cluster beam experiments. These calculations show that vanishing dipoles do not directly imply metallic behavior in the clusters. The question of the nature of the clusters thus remains unresolved.

In this paper we report the results of systematic DFT-based calculations of cluster polarizabilities over a wide size range from $N = 2$ to $N = 80$. By using a scheme that partitions the polarizability into site-specific contributions [11,12], we analyze the experimental polarizability results into charge transfer or metal-like contributions and local (dipole) or dielectriclike contributions. By considering the cluster-size trends of these contributions separately, we show that the behavior of the cluster polarizabilities is captured very well by a metal sphere model. We also show direct evidence of strong, metallic screening of atoms in the cluster interior from the effects of an applied electric field.

In the next section we review our site-specific methodology. We then present the main results of the calculations in Sec. III. In Sec. IV, we discuss and interpret the results. We close in Sec. V with a summary of the key findings.

*Corresponding author: mali@nwu.edu.cn
†Corresponding author: jacks1ka@cmich.edu
‡Corresponding author: jellinek@anl.gov

II. METHODOLOGY AND COMPUTATIONAL PROCEDURE

To insure physically meaningful results for calculated cluster properties, the correct atomic arrangements for the clusters must be used in the calculations. We determine the global minimum (GM) energy or ground-state structures of Na_N clusters using an unbiased, three-step search strategy similar to that used to successfully determine the ground-state structures of Cu clusters [13,14]. The method proceeds as follows at each cluster size. First, a large number of initial configurations is generated using the computationally efficient Gupta potential [15] and the basin-hopping algorithm encoded in the GMIN program [16]. Up to 200 basin-hopping runs are made at each size, each beginning from a different random starting structure. The 50 lowest energy structures produced in each run are saved and added to a database of candidate structures. Structures with energy differences of less than 10^{-5} eV are assumed to be identical, and duplicates are eliminated from the pool. Second, single-point DFT calculations are carried out at the geometries of the approximately 150 lowest energy local minima obtained in step 1. The resulting total energies (DFT1) are used to reorder the candidate structures. In the final step, the structures corresponding to the 20 lowest DFT1 energies are fully relaxed at the DFT level with no symmetry constraints. The lowest energy structure obtained in this step is assumed to be the GM for the given cluster size. Further discussion of the three-step search strategy can be found in Refs. [13] and [17].

All DFT calculations were carried out using the generalized gradient approximation of Perdew-Burke-Ernzerhof (PBE-GGA) [18] and an extensive, all-electron basis set formed from 16 bare Gaussians, including 6s-type, 4p-type, and 4d-type orbitals on each atom, as implemented in the NRLMOL code [19,20]. Recent studies indicate that the polarizability is well converged with a basis set of this quality [21]. Spin-polarized calculations were done for clusters with an odd numbers of electrons. Structural relaxations were done using a standard, gradient-based algorithm [22]. We estimate that the uncertainty in evaluating the total energies of the local minima to be no greater than 0.0015 Hartree or less than 0.05 eV using standard settings for NRLMOL.

The dipole polarizabilities of the ground-state structures were calculated using the site-specific partitioning method [11,12]. This scheme decomposes the total dipole moment and polarizability of a finite system exactly into nonoverlapping contributions from its constituent atoms. A complete description of the method can be found in Refs. [11] and [12]. Here we repeat only the details relevant to the discussion of the results.

The polarizabilityα of a system can be defined as

$$\alpha_{ij} = -\frac{d^2E}{dF_i dF_j}\bigg|_{F=0} \frac{\mathrm{d}\mu_i}{\mathrm{d}F_j}\bigg|_{F=0}, \tag{1}$$

where E is the total energy of the system, F is a uniform external electric field, and μ is the electric dipole of the system, and i and j label x, y, and z components. The dipole can be expressed as an integral over the cluster charge density. The integration volume can be partitioned over nonoverlapping atomic volumes Ω_A, each of which contains the nucleus of a single atom A. Ω_A is a Voronoi cell, i.e., the volume closer to A than to any other atom in the system. (Note that Ω_A can be generalized to represent the volume of a site that includes multiple atoms.) The integrals over Ω_A define the atomic dipole moments μ_i^A,

$$\mu_i^A = \int_{\Omega_A} r_i \rho(r) d^3r, \tag{2}$$

which sum exactly to the total dipole moment of the system:

$$\mu_i = \sum_A \mu_i^A. \tag{3}$$

The μ^A can be further partitioned into local dipole $\mu^{A,p}$ and charge transfer $\mu^{A,q}$ components

$$\mu_i^A = \mu_i^{A,p} + \mu_i^{A,q}, \tag{4}$$

where

$$\mu_i^{A,p} = \int_{\Omega_A} \left(r_i - R_i^A\right)\rho(r) d^3r, \tag{5}$$

and

$$\mu_i^{A,q} = \int_{\Omega_A} R_i^A \rho(r) d^3r = q^A R_i^A. \tag{6}$$

R^A is the position of the nucleus of atom A, and q^A is its net charge. $\mu^{A,p}$ represents the dipole moment of the total charge distribution in Ω_A with respect to R^A. Its value is clearly independent of the position of the origin of the overall coordinate system. $\mu^{A,q}$ is the dipole corresponding to a point charge of magnitude q^A located at R^A. Its value does depend on the choice of origin, except when $q^A = 0$, because R^A does. However, the sum of the $\mu^{A,q}$ over all atoms is origin independent for a neutral system.

Given the decomposition of the atomic dipole moment in Eq. (4), the atomic polarizability can be represented as

$$\alpha_{ij}^A = \alpha_{ij}^{A,p} + \alpha_{ij}^{A,q}, \tag{7}$$

with local dipole ($\alpha_{ij}^{A,p}$):

$$\alpha_{ij}^{A,p} = \frac{d\mu_i^{A,p}}{dF_j}\bigg|_{F=0}, \tag{8}$$

and charge transfer ($\alpha_{ij}^{A,q}$):

$$\alpha_{ij}^{A,q} = \frac{d\mu_i^{A,q}}{dF_j}\bigg|_{F=0} = R_i^A \frac{dq^A}{dF_j}\bigg|_{F=0} \tag{9}$$

components. $\alpha_{ij}^{A,p}$ reflects the change in the local dipole moment at site A when an external electric field is switched on. It is therefore sensitive to rearrangements of the electron charge density within Ω_A. $\alpha_{ij}^{A,q}$ reflects the change in the net site charge q^A when an external field is imposed. It is sensitive to transfers of charge between Ω_A and the rest of the cluster. Since $\alpha_{ij}^{A,p}$ and $\alpha_{ij}^{A,q}$ involve derivatives with respect to the *same* external field, comparing these quantities for different atoms directly indicates differences in how the charge density around those atoms changes due to the application of an external field. Summing the site-specific polarizabilities over all the atoms

and dividing by N leads to the total per atom local and charge transfer polarizabilities:

$$\frac{\alpha_{ij}^{p}}{N} = \frac{1}{N}\sum_{A}\alpha_{ij}^{A,p} \tag{10}$$

and

$$\frac{\alpha_{ij}^{q}}{N} = \frac{1}{N}\sum_{A}\alpha_{ij}^{A,q}. \tag{11}$$

As in the case of the corresponding dipole moments, each of the $\alpha_{ij}^{A,p}$ is independent of the choice of the origin, but $\alpha_{ij}^{A,q}$ is not. However, in a neutral system, α_{ij}^{q} does not depend on the location of the origin.

All polarizability components are evaluated using a finite difference method [23]. For a given cluster, a series of self-consistent DFT calculations are performed in which a small, uniform external electric field is oriented along the "+" and "−" x, y, and z directions, respectively. The polarizabilities are then calculated according to

$$\alpha_{i.j}^{A,p(q)} = \frac{\mu_i^{A,p(q)}(+F_j) - \mu_i^{A,p(q)}(-F_j)}{2F_j}, \tag{12}$$

where F_j is the magnitude of the external field applied in the jth coordinate direction. A magnitude of 0.005 atomic units for the external field has been found to yield numerically stable and well-converged results for the derivatives [23].

In the following sections, we mainly focus on isotropically averaged polarizabilities. For the sake of clarity, we use brackets to indicate the averaged values. For example,

$$\langle\alpha\rangle = \frac{1}{3}\sum_{i}\alpha_{ii}. \tag{13}$$

Also, it is convenient to introduce the following averaged quantity:

$$\left|\frac{dq^A}{dF}\right| = \sqrt{\left(\frac{dq^A}{dF_x}\right)^2 + \left(\frac{dq^A}{dF_y}\right)^2 + \left(\frac{dq^A}{dF_z}\right)^2}. \tag{14}$$

Its value is independent of the location of the origin of a given cluster, as are $\langle\alpha\rangle$, $\langle\alpha^p\rangle$, and $\langle\alpha^q\rangle$.

III. RESULTS

A. Ground-state structures and properties of Na_N clusters

We used the scheme described in Sec. II to obtain GM structures for Na_N (N = 2–30) clusters. The lowest energy structure found at each size is shown in Fig. 1. The clusters are planar for N = 3–5, while for N = 6–15 the structures are layered with no interior atoms. Na_{16} has one atom on what could be described as a concave surface site. For N = 17 and beyond, all clusters have at least one interior atom. For N = 17 and 18, the structures contain only one interior atom, while for N = 19–22 there are two, for N = 23 and 24 there are three, for N = 25–29 there are four, except for Na_{27}, which has five, and for Na_{30} there are six interior atoms. (Coordinates and other information regarding these cluster structures are available on request from the authors.)

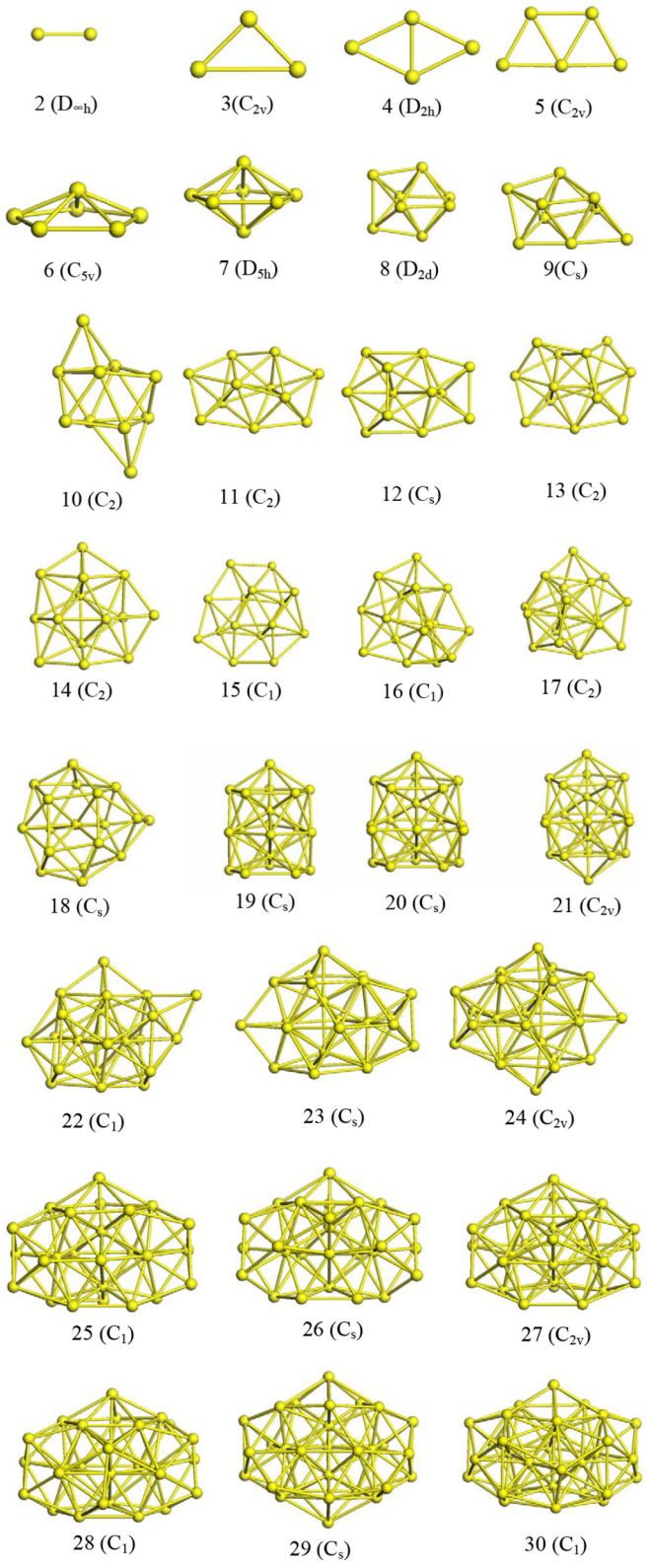

FIG. 1. (Color online) Ground-state structures of Na_N found using an unbiased search technique (N = 2–30).

There have been several earlier theoretical studies of the structures of Na_N clusters, especially for $N < 20$, but a few involving much larger structures [24–26]. A detailed review was given recently by Aguado and Kostko [26]. Here we

limit the comparison of the structures in Fig. 1 to the new results presented in Ref. [26]. Aguado and Kostko also carried out extensive, unbiased searches for Na_N GM structures for N up to 80 atoms. Their methodology also involves use of an empirical Gupta potential [15] and the basin-hopping algorithm [16] to create a large pool of candidate structures at each size. A subset of this pool was then chosen for study within DFT, in this case using the local spin density approximation (LSDA) [27]. To refine their pool, Aguado and Kostko [26] first grouped the Gupta-derived geometries based on shape characteristics and then chose the lowest energy isomer of each shape type for further studies. Their rationale for this procedure is that the energy ordering given by the empirical potential should be more reliable when comparing structures of similar overall shape. They also generated additional candidate structures by adding or removing single atoms to the low energy structures of a neighboring size. In total, up to 150 candidate structures were fully optimized at the LSDA level at each size.

We find a close agreement between the structures in Fig. 1 and those presented in Ref. [26] at all sizes up to $N = 30$. The proposed GM structures are the same for all sizes except for $N = 23$, 29, and 30. For Na_{23}, the structure in Fig. 1 coincides with the second-lowest structure reported in Ref. [26], which is nearly degenerate with their proposed GM. In our GGA-PBE calculations, the two structures are also nearly degenerate, separated by less than 0.03 eV. The ground-state structure for Na_{29} in Fig. 1 has C_s symmetry. It differs from the C_1 structure presented in Ref. [26] in the placement of a single cap atom. In GGA-PBE, the two structures are essentially degenerate, differing in total energy by less than 0.01 eV. The C_1 structure for Na_{30} shown in Fig. 1 also differs from the respective C_s structure in Ref. [26] by the placement of a single cap atom. At the GGA-PBE level, the C_s structure from Ref. [26] is 0.05 eV lower in energy than the structure shown in Fig. 1. The nearly exact agreement between the proposed GM structures presented in Ref. [26] and those found independently in this work (Fig. 1) demonstrates that unbiased search procedures can reliably locate the lowest energy cluster isomers.

In Fig. 2, we show structures for Na_N, $N = 38$, 40, 50, 55, 60, 70, and 80. These were taken from Ref. [26] and reoptimized using GGA-PBE. The resulting structures were used along with those in Fig. 1 to explore the trends of the cluster polarizability and other properties over a large range of cluster sizes. We now turn to those results.

In the upper panel of Fig. 3, we show the average bond length $\langle R \rangle$ as a function of cluster size. To determine $\langle R \rangle$ for a given cluster, bonds are assumed to exist between any two atoms separated by less than 1.25 $d_{\min}$, where $d_{\min}$ is the shortest interatomic separation in the cluster. This criterion was chosen by examining histograms of interatomic distances for several clusters. The histograms typically have a broad first peak that corresponds to first-neighbor separations. The bond criterion was chosen so as to include all of the bonds contributing to this peak when computing $\langle R \rangle$. For a typical cluster, 1.25 $d_{\min}$ is approximately 4.1 Å, well less than the distance to the second nearest neighbor in the bulk body-centered-cubic (bcc) structure for Na (4.2 Å).

$\langle R \rangle$ increases rapidly with N for the smallest clusters but reaches a maximum value of about 3.71 Å for $N = 80$.

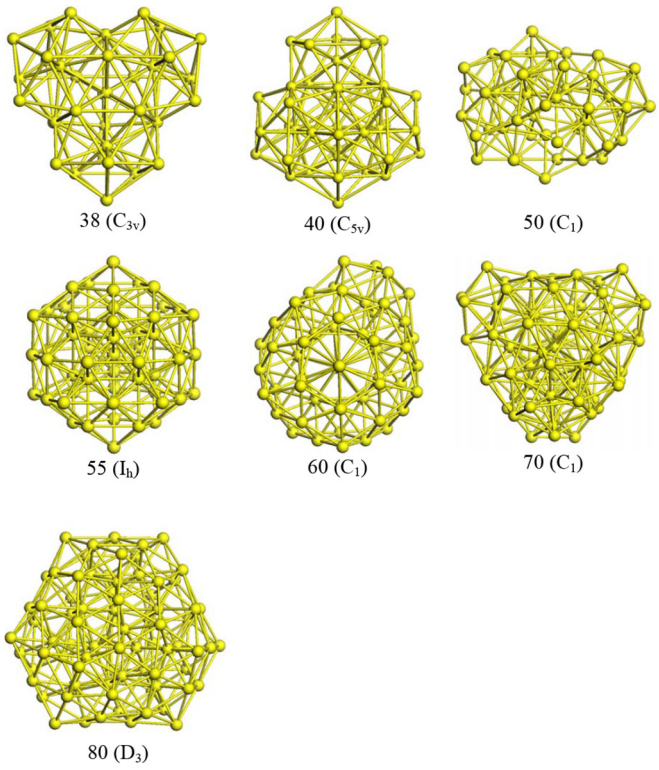

FIG. 2. (Color online) Ground state structures of Na_N ($N = 38$, 40, 50, 55, 60, 70, and 80) taken from Ref. [21] and reoptimized using GGA-PBE.

This is somewhat larger than the nearest-neighbor distance computed within PBE for the bulk sodium bcc lattice, 3.62 Å [4]. (For comparison, the experimentally determined bond length, measured at 5 K, is 3.659 Å [28].) As a rule, $\langle R \rangle$ increases with cluster size and approaches the bulk bond length from below at large values of N. The bcc structure of bulk Na is relatively open, and each atom has only eight nearest neighbors. The clusters have a more close-packed structure.

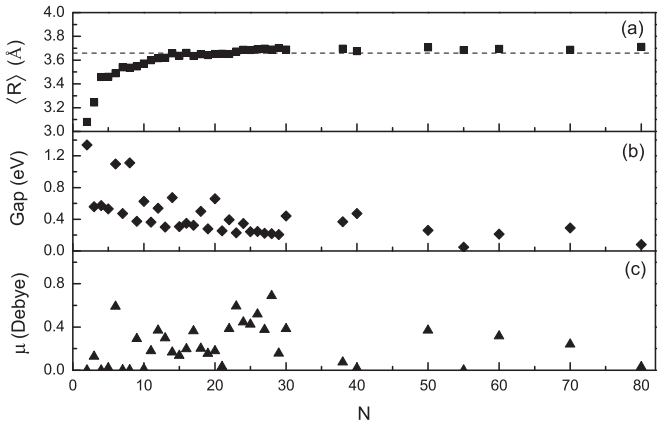

FIG. 3. Upper panel: Average nearest-neighbor distance $\langle R \rangle$ (in Å) vs N for the ground-state structures of Na_N clusters. The dashed line is the bulk Na bcc lattice nearest-neighbor distance, 3.659 Å [23]. Middle panel: HOMO-LUMO gap (in eV) vs N for ground state Na_N clusters. Lower panel: Computed electric dipole moments (in Debye) for ground state Na_N clusters.

For example, for $N = 70$ and 80, the average coordination is 8.5 and 8.9, respectively, even though many of the atoms are at the cluster surface. Generally, bond lengths increase with the number of nearest neighbors, so the somewhat larger cluster bond lengths appear to result from the fact that the cluster structures are more closely packed than the bcc bulk structure.

The energy gap between the highest occupied molecular orbital (HOMO) and lowest unoccupied molecular orbital (LUMO) is shown in the middle panel of Fig. 3. While HOMO-LUMO gaps are typically underestimated when computed in DFT using the corresponding Kohn-Sham eigenvalues, qualitative cluster size trends in the gap are reproduced [29]. In Fig. 3, the HOMO-LUMO gap for Na_N is seen to have a general trend toward smaller values as N increases, but there is considerable variation from cluster size to cluster size. At $N = 80$, the largest cluster considered here, the gap is 0.08 eV, yet at $N = 70$ the value is 0.29 eV. The HOMO-LUMO gap values are larger at sizes that correspond to electronic shell closures in a jellium model of the clusters (e.g., $N = 2$, 8, 18, and 20) [30].

As mentioned in the Introduction, the size of the dipole in Na clusters is a matter of significant current interest [7,9,10]. Recent experiments [7] suggested that permanent dipoles are vanishingly small in Na_N; however, DFT-based calculations [9,10] gave a different picture. They indicated that Na_N clusters have finite dipoles in their static, ground state geometries, but these average out to give nearly zero effective dipole moments when dynamical effects due to temperature and ZPM are taken into account.

We computed dipole moments (μ) for the static structures shown in Figs. 1 and 2. The results are shown in the bottom panel of Fig. 3. There is clearly significant variation in the value of μ with cluster size. Highly symmetric clusters such as Na_{55} have zero dipole moment, but lower symmetry structures such as Na_{60} have nonvanishing moments. The values are in good agreement with the recent results of Aguado *et al.* [9]. For example, for Na_{13} we obtain a value of 0.297 Debye compared to a value of 0.248 Debye given in Ref. [9] for the PBE density functional. We note that, as shown in Ref. [9], the computed value of the dipole moment for a given cluster size depends on the functional used for the calculation, but different functionals give similar qualitative comparisons between different cluster isomers and different cluster sizes.

B. Site-specific analysis of cluster polarizabilities

Site-specific polarizabilities have been computed for all of the clusters shown in Fig. 1 and Fig. 2 using the methodology described in Sec. II. For each cluster, values of $\langle \alpha^{A,p} \rangle$ and $\langle \alpha^{A,q} \rangle$ are computed for each atom A. Since $\langle \alpha^{A,q} \rangle$ depends on the choice of the origin of the coordinate system, it is more convenient to focus on the related quantity $|\frac{dq^A}{dF}|$, which is independent of this choice. As mentioned above, the site-specific polarizabilities indicate how the distribution of the charge density in the volume associated with that site (atom) changes when an electric field is applied. Specifically, $\langle \alpha^{A,p} \rangle$ is related to the change in the local dipole of atom A, and $|\frac{dq^A}{dF}|$ indicates how the net charge associated with atom A changes.

In Fig. 4, shading is used to show the magnitudes of $\langle \alpha^{A,p} \rangle$ and $|\frac{dq^A}{dF}|$ for the atoms in Na_6, Na_{14}, Na_{25}, and Na_{70}. The same shading scale is used for all cluster sizes, so a comparison between atoms can be made not only within a single cluster but also across the different clusters. For each quantity, the maximum value across all the clusters is used to define the darkest shading.

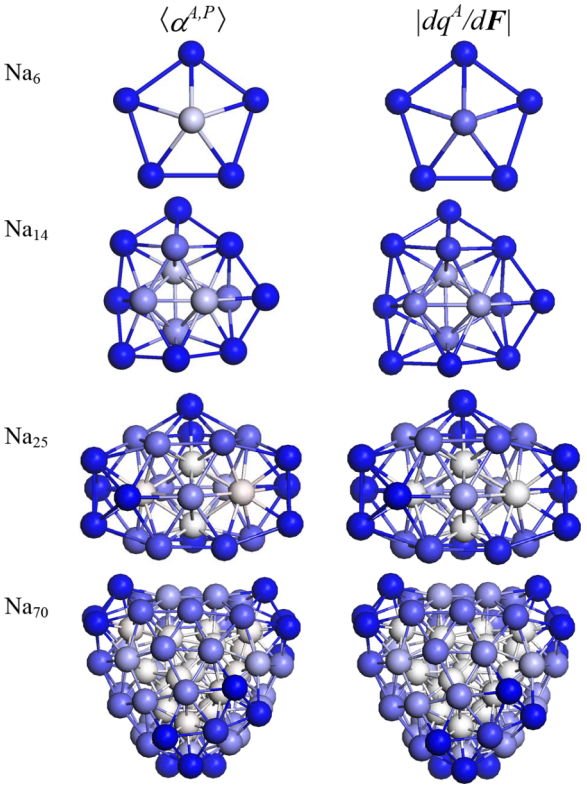

FIG. 4. (Color online) Site-specific values of $\langle \alpha^{A,p} \rangle$ and $|\frac{dq^A}{dF}|$ for Na_N, $N = 6$, 14, 25, and 70. The shading indicates the relative magnitudes of the quantities, with the darkest atoms having the largest values. The shading scale is set independently for each quantity, but the same scales are used for all four cluster sizes.

The same general behavior is exhibited by all the clusters in Fig. 4. The values of both $\langle \alpha^{A,p} \rangle$ and $|\frac{dq^A}{dF}|$ are smaller in magnitude for the atoms closer to the cluster center of mass than for atoms near the cluster surface. The difference is slightly more pronounced for $|\frac{dq^A}{dF}|$. In Na_{25} and Na_{70}, which have interior atoms, the values of both $\langle \alpha^{A,p} \rangle$ and $|\frac{dq^A}{dF}|$ for the interior atoms are close to zero. For Na_{25}, for example, the smallest magnitude of $\langle \alpha^{A,p} \rangle$ is 0.45 $Bohr^3$ for the interior atoms, while the largest value for an atom at the surface is about 57 $Bohr^3$. For $|\frac{dq^A}{dF}|$, the corresponding values are 0.35 and 38 $Bohr^2$. Some of the values of $\langle \alpha^{A,p} \rangle$ and $\langle \alpha^{A,q} \rangle$ for interior atoms have a negative sign. This indicates that, for a given applied field, the dipoles induced in these atomic volumes are opposite in direction to the applied field.

To show the trends differently, the values of $\langle \alpha^{A,p} \rangle$ (squares) and $|\frac{dq^A}{dF}|$ (circles) are plotted as a function of the distance of the various atoms from the center of mass of the clusters in Fig. 5. As mentioned, the trends for both quantities are very similar in all the clusters. Reading from right to left in each panel clearly shows that the atoms furthest from the cluster center generally have the largest values and that the values

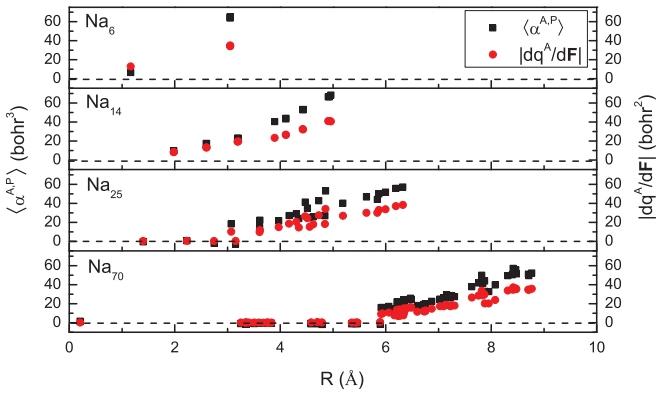

FIG. 5. (Color online) Site-specific values of $\langle\alpha^{A,p}\rangle$ and $|\frac{dq^A}{dF}|$ vs distance of atom A from the cluster center of mass (R), for Na_N, $N = 6$, 14, 25, and 70.

decrease to approximately zero for atoms in the cluster interior. (There are no true interior atoms in Na_6 or Na_{14}. While Na_6 is quasiplanar, the central atom lies above the plane defined by the pentagon.) The maximum values of $\langle\alpha^{A,p}\rangle$ and $|\frac{dq^A}{dF}|$ for the surface atoms are similar for all of the clusters. $\langle\alpha^{A,p}\rangle$ and $|\frac{dq^A}{dF}|$ span a range of values over the various surface atoms. This corresponds to the differences in shading seen for the surface atoms in Fig. 4.

The evolution of $\frac{\langle\alpha\rangle}{N}$, $\frac{\langle\alpha^q\rangle}{N}$, and $\frac{\langle\alpha^p\rangle}{N}$ with N is shown in Fig. 6; the values of these quantities are independent of the location of the origin of the system of coordinates. For comparison, measured values for $\frac{\langle\alpha\rangle}{N}$ obtained by Bowlan *et al.* in recent experiments [7] are also shown. The calculated and experimentally determined values exhibit the same trends with cluster size, although the calculated values are shifted down from the experimentally determined values by a roughly constant amount of 10.0 Bohr^3. We discuss this difference further below. The values of $\frac{\langle\alpha^p\rangle}{N}$ follow a smoothly decreasing

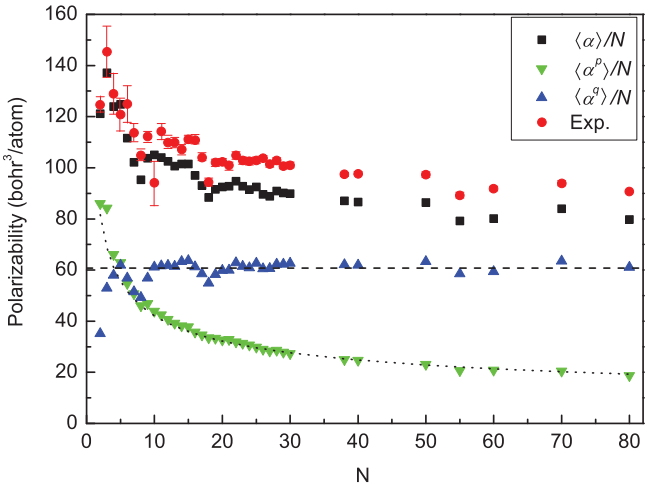

FIG. 6. (Color online) Isotropic per atom polarizabilities $\langle\alpha\rangle/N$, $\langle\alpha^p\rangle/N$, and $\langle\alpha^q\rangle/N$ for Na_N clusters vs N. The bulk polarizability per atom is shown by the dashed line and has the value 60.75 Bohr^3/atom. The dotted line is a plot of the second two terms on the right side of Eq. 23, with $\delta = 0.86$ Å.

trend with cluster size. By contrast, the values of $\frac{\langle\alpha^q\rangle}{N}$ undergo significant fluctuations at the smallest sizes but reach a roughly constant value beyond $N = 20$. The fluctuations in the values of $\frac{\langle\alpha\rangle}{N}$ are largely due to the fluctuations in $\frac{\langle\alpha^q\rangle}{N}$.

To characterize the anisotropy in the response of a cluster to the direction of the applied external electric field, we define the polarizability anisotropy η as

$$\eta = \frac{\alpha_1 - \alpha_3}{\langle\alpha\rangle}, \tag{15}$$

where α_k ($k = 1, 2, 3$) are the eigenvalues of the total polarizability matrix, labeled so that $\alpha_1 \geqslant \alpha_2 \geqslant \alpha_3$. Physically, the eigenvectors of the polarizability matrix define those directions in which the change in the dipole moment of a system in response to an external electric field is simply a scaling by a scalar factor, and the eigenvalues reflect the rate of change of the dipole moment with the field in the limit of vanishingly small field.

The polarizability eigenvalues can be decomposed into local (or dipole) α_k^p and charge transfer α_k^q contributions:

$$\alpha_k = \alpha_k^p + \alpha_k^q, \tag{16}$$

where α_k^p and α_k^q are the diagonal elements of the local (or dipole) α^p and charge transfer α^q matrices subjected to the same transformation that diagonalizes the total polarizability matrix α. (Note that α^p and α^q are not themselves diagonalized by this transformation. See Ref. [10] for further discussion.) Given this, η can be partitioned into local (or dipole) η^p and charge transfer η^q contributions:

$$\eta = \eta^p + \eta^q, \tag{17}$$

where

$$\eta^p = \frac{\alpha_1^p - \alpha_3^p}{\langle\alpha\rangle} \tag{18}$$

and

$$\eta^q = \frac{\alpha_1^q - \alpha_3^q}{\langle\alpha\rangle}. \tag{19}$$

The polarizability anisotropies and their dipole and charge transfer components for Na_N clusters are plotted in Fig. 7. It is clear from the figure that η is dominated by η^q for all clusters. The implication is that the directional dependence of the polarizability is carried mainly through the charge transfer component. The values of η^p are much smaller at all sizes. This implies that the change in the local dipole part of the cluster dipole moment due to an external electric field is nearly the same regardless of the direction of the field. The sign of η^p is negative for many clusters. This indicates that the dipole part of the total polarizability of these clusters is largest in a direction other than that for the charge transfer part.

To connect the polarizability anisotropy to cluster shape, we define a shape anisotropy χ as

$$\chi = \frac{I_3 - I_1}{\langle I\rangle}, \tag{20}$$

where I_k ($k = 1, 2, 3$) are the principal moments of inertia of the cluster labeled so that $I_1 \leqslant I_2 \leqslant I_3$ and $\langle I\rangle = (I_3 + I_2 + I_1)/3$. Note that this numbering scheme is opposite to the convention used for α_1, α_2, and α_3. In general, systems

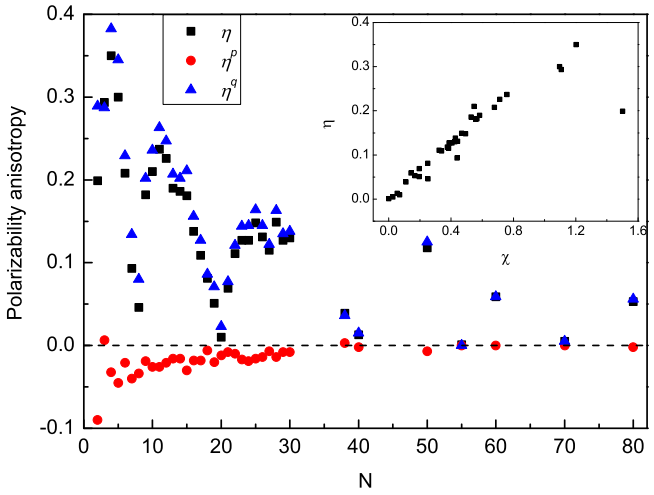

FIG. 7. (Color online) Polarizability anisotropies η, η^p, and η^q for Na_N vs N. Inset: Correlation between the cluster polarizability anisotropy η and the shape anisotropy χ for Na_N. See text for details.

are most polarizable along the direction of their largest linear dimension. But the moment of inertia with respect to an axis that points in this direction is the smallest. With reversed numbering schemes for the polarizabilities and the moments of inertia, the eigenvectors that correspond to the eigenvalues of these two quantities with the same k define the same or nearly the same spatial directions.

We show a plot of η vs χ for all the clusters in the inset of Fig. 7. There is a strong correspondence between η and χ, showing that the clusters with the most (least) isotropic mass distributions (i.e., the ones that are the most (least) spherical) also have the most (least) isotropic polarizabilites. This correlation between the polarizability anisotropy η and the shape anisotropy χ can be rationalized by noting that η is dominated by η^q, and that the atomic contributions $\alpha_{ij}^{A,q}$ defining η^q depend on the atomic positions R_i^A (Eq. 9).

IV. DISCUSSION

A simple model expresses the polarizability of a metal sphere [6,31,32] as

$$\langle\alpha\rangle = (R+\delta)^3, \tag{21}$$

where R is the sphere radius and δ is a parameter representing the distance that the electron charge density extends beyond the sphere radius due to the finite decay length of the electron wave functions. In the context of an atomic cluster, R can be thought of as the typical distance from the cluster center to the nucleus of a surface atom. δ then represents an appropriate average distance beyond the nucleus that the valence electron charge density extends. In the limit of a macroscopic sphere, δ can be neglected, and the bulk polarizability per atom (α_0) can be expressed in terms of the volume per atom (V_0) of the sphere:

$$\alpha_0 = \frac{R^3}{N} = \frac{3}{4\pi}V_0. \tag{22}$$

Using the experimental value of the bulk bcc unit cell parameter (4.225 Å) [28], we obtain $\alpha_0 = 60.75$ Bohr^3. Multiplying the cube in Eq. 21 and using Eq. 22 to replace R by $(N\alpha_0)^{1/3}$, we obtain

$$\left\langle\frac{\alpha}{N}\right\rangle = \alpha_0 + 3\alpha_0^{2/3}\delta N^{-1/3} + 3\alpha_0^{1/3}\delta^2 N^{-2/3}, \tag{23}$$

where we have dropped the δ^3 term, which can be shown to be negligible for all but the smallest clusters (see below).

Before using Eq. 23 to interpret the trends in Fig. 6, it is worth considering a simple scaling argument [12] regarding the expected behavior of $\frac{\langle\alpha^q\rangle}{N}$ and $\frac{\langle\alpha^p\rangle}{N}$ with size. As can be seen in Figs. 4 and 5, both $\frac{\langle\alpha^q\rangle}{N}$ and $\frac{\langle\alpha^p\rangle}{N}$ are dominated by contributions from the cluster surface. In the presence of an external field, the induced surface charge on a cluster is proportional to σR^2, where the surface charge density, σ, is proportional to the external field strength. The charge transfer dipole will then scale as σR^3, where the additional factor of R is the distance of the induced charge to the cluster center (cf. Eq. 9). $\frac{\langle\alpha^q\rangle}{N}$ can therefore be expected to be constant with size since R^3 is proportional to the cluster volume and, therefore, to N. The local dipole is also dominated by surface contributions, but the local dipole for the surface atoms scales as $\sigma R^2 d$, where d represents the distance between the induced surface charge and the nuclei of the surface atoms. Thus, $\frac{\langle\alpha^p\rangle}{N}$ could be expected to fall off like $1/R$ or $N^{-1/3}$ to leading order.

Turning to the results shown in Fig. 6, it is clear that $\frac{\langle\alpha^q\rangle}{N}$ is roughly constant for large cluster sizes, as expected from the scaling argument. Its value fluctuates about α_0, which is indicated in the figure by the dashed line. Thus, the size-independent term in Eq. 23 can be identified with $\frac{\langle\alpha^q\rangle}{N}$. The remaining terms can therefore be related to $\frac{\langle\alpha^p\rangle}{N}$. By assuming δ to be constant and varying its value, we obtain a best fit to the computed values of $\frac{\langle\alpha^p\rangle}{N}$, shown by the dotted curve in Fig. 6. The fit is extremely good and corresponds to $\delta =$ 1.63 Bohr, or 0.86 Å. This is approximately $\frac{1}{4}$ of the average nearest-neighbor separation of 3.7 Å for the Na atoms in the clusters.

It is interesting to note that the δ^2 term in Eq. 23 is sizable throughout the range of clusters sizes shown in Fig. 6 and cannot be neglected from the fit. For example, at $N = 16$ this term has a magnitude of about 6 Bohr^3 or about 20% of the value of $\frac{\langle\alpha^p\rangle}{N}$ at this size. By $N = 80$, the δ^2 term has decreased to about 1.7 Bohr^3, but this remains about 9% of $\frac{\langle\alpha^p\rangle}{N}$. At still larger sizes, the relative contribution of the δ^2 term to $\frac{\langle\alpha^p\rangle}{N}$ decreases further and can ultimately be neglected in comparison to the linear term. By contrast, the δ^3 term neglected in Eq. 23 has a value of 2.17 Bohr^3 at $N = 2$ or only 2.5% of the total value of $\frac{\langle\alpha^p\rangle}{N}$. Its relative contribution falls off quickly for larger sizes. For this reason it can be dropped from Eq. 23.

The degree to which the terms in Eq. 23 capture the size-dependent trends in $\frac{\langle\alpha^q\rangle}{N}$ and $\frac{\langle\alpha^p\rangle}{N}$ is striking. It is essentially only the dips in $\frac{\langle\alpha^q\rangle}{N}$ near $N = 2$, 8, and 18 that are not reproduced. These coincide with jellium shell closings corresponding to filling the $1S$, $1P$, and $1D$ shells, respectively [30]. Such clearly quantum mechanical effects are outside the essentially classical domain of the model. Discounting these, the metal sphere model clearly describes the behavior of the Na clusters very well.

The results shown in Figs. 4 and 5 are also consistent with a metallic model. The fact that both $\langle \alpha^{A,p} \rangle$ and $|\frac{dq^A}{dF}|$ are close to zero for the interior atoms in the Na clusters implies that there is little charge induced on these atoms by an external field; therefore, the interior atoms are strongly shielded from the effects of an external field. In the limit of the bulk metal, the shielding is complete and $\langle \alpha^{A,p} \rangle$ and $|\frac{dq^A}{dF}|$ would be exactly zero for interior atoms. The behavior seen in Figs. 4 and 5 for the clusters coincides qualitatively very well with this picture.

In Fig. 6 we compare the calculated values for $\frac{\langle \alpha \rangle}{N}$ to the corresponding experimental values [7]. The calculated values track the size-related trends in the experimental values extremely well, reproducing essentially all of the features, including the large dips related to shell closings ($N = 2$, 8, 18) as well as the smaller fluctuations at larger sizes. For Na and Na_2, the agreement between calculated and measured values is quantitative (159.16 and 122.5 vs 160.4 and 124.9 $Bohr^3$/atom, respectively). However, for other sizes the calculated $\frac{\langle \alpha \rangle}{N}$ values are consistently smaller than the experimental values. The only exceptions are for $N = 5$ and $N = 10$, for which the calculated values (124.8 and 99.9 $Bohr^3$/atom) are somewhat larger than the experimental values (120.7 and 94.1 $Bohr^3$/atom). Of note is the fact that the difference is approximately constant with size. Between $N = 11$ and 80, the average difference between the calculated and measured values is 10.2 $Bohr^3$/atom, with a standard deviation of only 1.8 $Bohr^3$/atom.

The constancy of this difference deserves attention in light of the decomposition of $\frac{\langle \alpha \rangle}{N}$ into $\frac{\langle \alpha^q \rangle}{N}$ and $\frac{\langle \alpha^p \rangle}{N}$ shown in Fig. 6 and discussed previously. The fact that $\frac{\langle \alpha^q \rangle}{N}$ is essentially constant, while $\frac{\langle \alpha^p \rangle}{N}$ depends strongly on N, suggests that the difference must be related to $\frac{\langle \alpha^q \rangle}{N}$, yet the calculated limiting value of $\frac{\langle \alpha^q \rangle}{N}$ agrees with the expected bulk value. At the same time, the size dependence of $\frac{\langle \alpha^p \rangle}{N}$ is exactly as expected from the form of Eq. 23. Why, then, is the sum of $\frac{\langle \alpha^q \rangle}{N}$ and $\frac{\langle \alpha^p \rangle}{N}$ not equal to the measured values?

The difference between the computed and measured values of $\frac{\langle \alpha \rangle}{N}$ cannot be attributed simply to an inadequacy of the computational framework (the exchange correlation functional, the basis set, etc.). As noted above, the theory reproduces the measured values of α very well for Na and Na_2, and the nearly constant value of $\frac{\langle \alpha^q \rangle}{N}$ agrees well with the value expected from the bulk. A different theory-related problem has to do with calculated PBE-GGA bond lengths. The PBE-GGA bond length for bcc Na is 3.62 Å [4], compared to the low-temperature experimental value of 3.66 Å, an underestimate of about 1%. If cluster bond lengths were similarly underestimated, the radius of a given cluster would be underestimated by 1% and the corresponding value of $\frac{\langle \alpha^q \rangle}{N}$ by about 3%, or about 2 $Bohr^3$/atom. This is much smaller than the difference seen in Fig. 6. Furthermore, the calculated bond length for Na_2, 3.09 Å, is in close agreement with the corresponding experimental value, 3.08 Å [33]. This suggests that the calculated cluster bond lengths may actually be closer to the true bond lengths than would be expected from the bulk comparison. Based on these considerations, it appears clear that the theory-experiment difference seen in Fig. 6 cannot be due to poor theoretical bond lengths.

Another possible source of the difference is related to temperature. Since the radius of a cluster increases with temperature due to thermal expansion, the cluster's polarizability could be expected to increase as well. The measured polarizability therefore depends on the temperature of the cluster in the experiment. The calculated value, by contrast, is computed for ground state structures that correspond to $T = 0$. Several groups have investigated this effect [4,34–37]. Kronik *et al.* [4,36], and later Gamboa *et al.* [37], carried out DFT-based MD simulations to show directly that the computed values of $\frac{\langle \alpha \rangle}{N}$ for clusters indeed increase with temperature. However, the cluster temperatures in the experiments that yielded the data shown in Fig. 6 were reported [7] to be 20 K. Using the results of Gamboa *et al.* [37] as a guide, we estimate that the increase in $\frac{\langle \alpha \rangle}{N}$ for clusters at this low temperature would be well less than 1 $Bohr^3$/atom. In addition, the results of Ref. [37] indicate that the same increase in temperature can give very different increases in the polarizability per atom for clusters of different size. Thus, the temperature effect is not consistent with a constant difference between computed and measured values as seen in Fig. 6, assuming all clusters to have the same temperature in the experiment.

Recently, Aguado *et al.* [10] used a van der Waals (vdW) corrected DFT (vdW-DFT) [38] to study Na_N structures between $N = 10$ and 20. They reported that the energetic ordering of cluster isomers was somewhat different in vdW-DFT than in PBE-GGA and resulted in different GM structures at some sizes. They also reported that values of $\frac{\langle \alpha \rangle}{N}$ computed in vdW-DFT are somewhat larger than in PBE-GGA. Comparing directly, we find the results in Ref 10 to be 2–3 $Bohr^3$/atom larger on average than our results for this size range. While this is the right direction to explain the discrepancy with experiment, it does not explain the full difference.

Aguado *et al.* [10] also considered the effect of quantum ZPM on calculated polarizabilities. As noted in the Introduction, this was done by carrying out DFT-based MD simulations for the clusters. The MD runs were started by placing an amount of energy equal to the corresponding quantum zero point energy into each vibrational degree of freedom for the cluster. By averaging polarizabilities computed for several configurations selected from the MD run, an average increase of 2–3 $Bohr^3$/atom over the value of the polarizability for the GM structure was found for the clusters in the range $N = 10$–20. Again, this is too small to account for the full theory-experiment difference. (Note that a change of this magnitude added to our results for $\frac{\langle \alpha^q \rangle}{N}$ would not seriously impact the agreement with α_0.)

While none of the effects considered above is large enough to account for the difference between the computed and measured values of $\frac{\langle \alpha \rangle}{N}$ seen in Fig. 6, it is possible that more than one of these effects could combine to explain the difference. It may also be possible that a systematic downward shift in the experimental values of $\frac{\langle \alpha \rangle}{N}$, as deduced from the beam deflection measurements, is an additional reason for the theory-experiment difference.

Finally, we return to the near constancy of $\frac{\langle \alpha^q \rangle}{N}$ and its agreement with the value for bulk Na. The remarkable result is that the per atom polarizability of bulk sodium is already present in Na clusters down to the smallest sizes studied here.

This is true despite the fact that nonmetallic characteristics are also present in these clusters. For example, the HOMO-LUMO gaps of the smallest clusters (Fig. 3) are quite large, ranging up to 1 eV. The contribution of $\frac{\langle\alpha^p\rangle}{N}$ to $\frac{\langle\alpha\rangle}{N}$ is significant over the range of Fig. 6 and vanishes gradually at larger sizes, revealing ever more clearly the metallic character inherent in the clusters from the smallest sizes as $\frac{\langle\alpha\rangle}{N}$ reaches the proper bulk limit. We conjecture that the trend-exhibited behavior by the $\frac{\langle\alpha^p\rangle}{N}$ and $\frac{\langle\alpha^q\rangle}{N}$ graphs of Fig. 6 for $\frac{\langle\alpha^q\rangle}{N}$ are generic to all elements that are metals in bulk quantities. Preliminary results for Cu and K clusters support this conjecture: The values of $\frac{\langle\alpha^q\rangle}{N}$ for these systems are near the corresponding bulk values already at small sizes and fluctuate about it as the clusters grow in size, whereas the values of $\frac{\langle\alpha^p\rangle}{N}$ decrease with the increase in the cluster size. The implications of the above conjecture are that the values/behavior of $\frac{\langle\alpha^p\rangle}{N}$ and $\frac{\langle\alpha^q\rangle}{N}$ as exhibited by clusters of even small sizes can serve as a predictive descriptor of whether an element, when in bulk quantities, is a metal or nonmetal. In that, $\frac{\langle\alpha^q\rangle}{N}$ and $\frac{\langle\alpha^p\rangle}{N}$ are different from many other descriptors/properties. For example, to predict the bulk lattice structure, one needs to consider clusters of much larger sizes, typically containing thousands or even tens of thousands of atoms.

V. SUMMARY

In this paper we presented the results of extensive, unbiased searches for the ground-state structures of Na_N, with $N = 3$–30. The structures we report reproduce almost exactly those found independently by Aguado and Kostko [26], demonstrating that careful, unbiased searches can be used to locate GM energy structures. We then studied the polarizabilities of the clusters, including structures at $N = 38$, 40, 50, 55, 60, 70, and 80 taken from Ref. [26], to elucidate trends out to large cluster sizes. The polarizabilities are calculated using an analysis scheme that partitions the total cluster polarizability, $\frac{\langle\alpha\rangle}{N}$, exactly into site-specific contributions. The individual atomic polarizabilities are then further decomposed into local (or dipole) and charge-transfer components that can be summed to give the total charge transfer $\frac{\langle\alpha^q\rangle}{N}$ and dipole $\frac{\langle\alpha^p\rangle}{N}$ polarizabilities for the clusters. Each of these quantities is independent of the choice of origin of the cluster and represents a metallicklike and a dielectriclike response of the cluster, respectively.

The results indicate strong electrostatic screening of the cluster interior from the effects of an applied field. The individual site-specific polarizabilities are large for atoms at surface sites and close to zero for interior sites. This screening is characteristic of metallic behavior in the clusters. In fact, a simple model based on the polarizability of a metal sphere is shown to capture the size trends of the cluster polarizability and its local dipole and charge transfer contributions over the entire size range studied here. Remarkably, the calculated values of $\frac{\langle\alpha^q\rangle}{N}$ attain an approximately constant value equal to the bulk limit already at very small cluster sizes, indicating that clear metallic character is present even in the smallest clusters and does not grow in with cluster size.

The decomposition of the cluster polarizability into site-specific contributions allows unique insight into the behavior of condensed matter at the smallest length scales. As Figs. 4 and 5 indicate, the analysis can be used to directly probe electrostatic screening and therefore to address questions related to the metallic character of a system. Such questions about nanoscale matter are of fundamental, as well as growing technological, interest. We expect that application of the site-specific methodology to additional cluster systems will help to develop a more robust understanding of nanoscale metallicity.

ACKNOWLEDGMENTS

We are grateful to Dr. Andres Aguado for providing us with structures for the larger Na clusters. We also benefitted from discussions with Prof. L. C. Balbas regarding the nature of Na clusters. K.A.J. is grateful for the hospitality of the University of Minnesota School of Physics and Astronomy, and particularly that of Prof. Ken Heller, during his sabbatical leave. Most of the calculations described in this work were performed at the HPCC at Michigan State University. M.L. was supported by the National Natural Science Foundation of China (Grant No. 11204240), the Research Fund for the Doctoral Program of Higher Education of China (Grant No. 20126101120023), the Scientific Research Projects of Shaanxi Provincial Department of Education (Grant No. 12JK0956), and the Technology Foundation for Selected Overseas Chinese Scholar. K.A.J. was supported by the US Department of Energy Grant No. DE-SC0001330. J.J. was supported by the Office of Basic Energy Sciences, Division of Chemical Sciences, Geosciences and Biosciences, US Department of Energy under Contract No. DE-AC02-06CH11357. M.H. acknowledges U.S. National Science Foundation Grant No. PHY-1068217.

[1] W. D. Knight, K. Clemenger, W. A. de Heer, and W. A. Saunders, Phys. Rev. B **31**, 2539 (1985).
[2] W. A. de Heer, Rev. Mod. Phys. **65**, 611 (1993).
[3] I. Moullet, J. L. Martins, F. Reuse, and J. Buttet, Phys. Rev. B **42**, 11598 (1990).
[4] L. Kronik, I. Vasiliev, M. Jain, and J. R. Chelikowsky, J. Chem. Phys. **115**, 4322 (2001).
[5] S. Kümmel, T. Berkus, P.-G. Reinhard, and M. Brack, Eur. Phys. J. D **11**, 239 (2000).
[6] J. Guan, M. E. Casida, A. M. Köster, and D. R. Salahub, Phys. Rev. B **52**, 2184 (1995).
[7] J. Bowlan, A. Liang, and W. A. de Heer, Phys. Rev. Lett. **106**, 043401 (2011).
[8] I. A. Solov'yov, A. V. Solov'yov, and W. Greiner, Phys. Rev. A **65**, 053203 (2002).
[9] A. Aguado, A. Largo, A. Vega, and L. C. Balbás, Chem. Phys. **399**, 252 (2012).
[10] A. Aguado, A. Vega, and L. C. Balbás, Phys. Rev. B **84**, 165450 (2011).

[11] K. Jackson, M. Yang, and J. Jellinek, J. Phys. Chem. C **111**, 17952 (2007).
[12] K. Jackson, L. Ma, M. Yang, and J. Jellinek, J. Chem. Phys. **129**, 144309 (2008).
[13] M. Yang, K. Jackson, C. Koehler, T. Frauenheim, and J. Jellinek, J. Chem. Phys. **124**, 024308 (2006).
[14] M. Jiang, Q. Zeng, T. Zhang, M. Yang, and K. A. Jackson, J. Chem. Phys. **136**, 104501 (2012).
[15] R. P. Gupta, Phys. Rev. B **23**, 6265 (1981).
[16] D. J. Wales and J. P. K. Doye, J. Phys. Chem. A **101**, 5111 (1997).
[17] M. Horoi and K. Jackson, Chem. Phys. Lett. **427**, 147 (2006).
[18] J. P. Perdew, K. Burke, and M. Ernzerhof, Phys. Rev. Lett. **77**, 3865 (1996).
[19] M. R. Pederson and K. A. Jackson, Phys. Rev. B **41**, 7453 (1990).
[20] K. A. Jackson and M. R. Pederson, Phys. Rev. B **42**, 3276 (1990).
[21] F. A. L. de Souza and F. E. Jorge, J. Braz. Chem. Soc. **24**, 1357 (2013).
[22] D. C. Liu and J. Nocedal, Math. Prog. **45**, 503 (1989).
[23] D. Porezag and M. R. Pederson, Phys. Rev. B **54**, 7830 (1996).
[24] S. M. Ghazi, S. De, D. G. Kanhere, and S. Goedecker, J. Phys. Cond. Matt. **23**, 405303 (2011)
[25] O. Kostko, B. Huber, M. Moseler, and B. von Issendorff, Phys. Rev. Lett. **98**, 043401 (2007); B. Huber, M. Moseler, O. Kostko, and B. von Issendorf, Phys. Rev. B **80**, 235425 (2009).
[26] A. Aguado and O. Kostko, J. Chem. Phys. **134**, 164304 (2011).
[27] J. P. Perdew and A. Zunger, Phys. Rev. B **23**, 5048 (1981).
[28] C. Kittel, *Introduction to Solid State Physics*, 8th ed. (Wiley, New York, 2004).
[29] S. Ishii, K. Ohno, Y. Kawazoe, and S. G. Louie, Phys. Rev. B **63**, 155104 (2001).
[30] M. Brack, Rev. Mod. Phys. **65**, 677 (1993).
[31] D. E. Beck, Phys. Rev. B **30**, 6935 (1984).
[32] D. R. Snider and R. S. Sorbello, Phys. Rev. B **28**, 5702 (1983).
[33] K. P. Huber and G. Herzberg, *Molecular Spectra and Molecular Structure: IV. Constants of Diatomic Molecules* (Van Nostrand, New York, 1979).
[34] S. Kümmel, J. Akola, and M. Manninen, Phys. Rev. Lett. **84**, 3827 (2000).
[35] S. A. Blundell, C. Guet, and R. R. Zope, Phys. Rev. Lett. **84**, 4826 (2000).
[36] L. Kronik, I. Vasiliev, and J. R. Chelikowsky, Phys. Rev. B **62**, 9992 (2000).
[37] G. U. Gamboa, P. Calaminici, G. Geudtner, and A. M. Köster, J. Phys. Chem. A **112**, 11969 (2008).
[38] M. Dion, H. Rydberg, E. Schröder, D. C. Langreth, and B. I. Lundqvist, Phys. Rev. Lett. **92**, 246401 (2004).